

Structural Effects of Gas Hydrate Antiagglomerant Molecules on Interfacial Interparticle Force Interactions

Sijia Hu, Loan Vo, Deepak Monteiro, Scot Bodnar, Philippe Prince, and Carolyn A. Koh*

Cite This: *Langmuir* 2021, 37, 1651–1661

Read Online

ACCESS |



Metrics & More

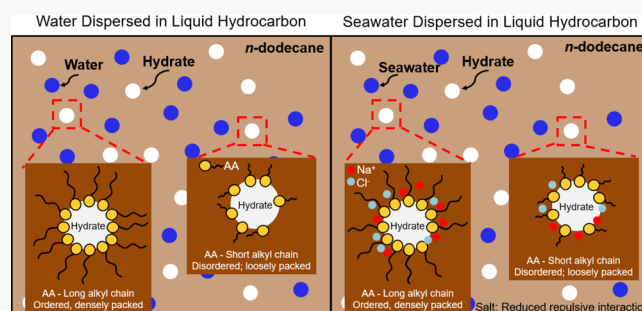


Article Recommendations



Supporting Information

ABSTRACT: Gas hydrate interparticle cohesive forces are important to determine the hydrate crystal particle agglomeration behavior and subsequent hydrate slurry transport that is critical to preventing potentially catastrophic consequences of subsea oil/gas pipeline blockages. A unique high-pressure micromechanical force apparatus has been employed to investigate the effect of the molecular structure of industrially relevant hydrate antiagglomerant (AA) inhibitors on gas hydrate crystal interparticle interactions. Four AA molecules with known detailed structures [quaternary ammonium salts with two long tails (R1) and one short tail (R2)] in which the R1 has 12 carbon (C12) and 8 carbon (C8) and saturated (C–C) versus unsaturated (C=C) bonding are used in this work to investigate their interfacial activity to suppress hydrate crystal interparticle interactions in the presence of two liquid hydrocarbons (*n*-dodecane and *n*-heptane). All AAs were able to reduce the interparticle cohesive force from the baseline ($23.5 \pm 2.5 \text{ mN m}^{-1}$), but AA-C12 shows superior performance in both liquid hydrocarbons compared to the other AAs. The interfacial measurements indicate that the AA with an R1 longer alkyl chain length can provide a denser barrier, and the AA molecules may have higher packing density when the AA R1 alkyl tail length is comparable to that of the liquid hydrocarbon chain on the gas hydrate crystal surface. Increasing the salinity can promote the effectiveness of an AA molecule and can also eliminate the effect of longer particle contact times, which typically increases the interparticle cohesive force. This work reports the first experimental investigation of high-performance known molecular structure AAs under industrially relevant conditions, showing that these molecules can reduce the interfacial tension and increase the gas hydrate–water contact angle, thereby minimizing the gas hydrate interparticle interactions. The structure–performance relation reported in this work can be used to help in the design of improved AA inhibitor molecules that will be critical to industrial hydrate crystal slurry transport.



INTRODUCTION

Gas hydrates belong to a class of compounds commonly known as clathrates. Gas hydrates are crystalline inclusion compounds composed of a three-dimensional lattice of hydrogen-bonded water and gas molecules (e.g., methane, ethane, carbon dioxide, etc.) formed under high-pressure and low-temperature conditions.^{1,2} Gas molecules with appropriate sizes can fit into the water cages of the hydrate structure. Gas hydrates are classified into three crystal structures: cubic structure I (sI), cubic structure II (sII), and hexagonal structure (sH).¹ Figure 1 shows the typical structures of sI hydrates with small dodecahedral and large tetradecahedral water cages.

Gas hydrates potentially provide a significant resource of energy and have promising applications in energy recovery and gas storage,^{3–5} because of their wide occurrence in deep ocean sediments and permafrost environments and storage density of around 164 volumes of gas per volume of hydrate, respectively.^{6–9} However, gas hydrates can be formed in subsea oil and gas flowlines because their operating conditions include the high-pressure and low-temperature conditions at

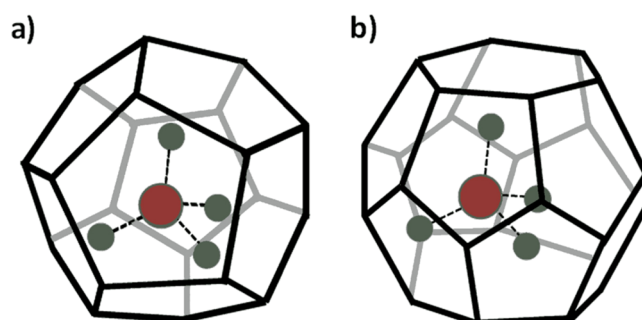


Figure 1. Conceptual illustration of (a) small dodecahedral and (b) large tetradecahedral water cages for structure I (sI) hydrates with a methane molecule occupying the cavity.¹

Received: August 23, 2020

Revised: January 12, 2021

Published: January 28, 2021



which gas hydrates are thermodynamically stable.¹ The formation, agglomeration, and deposition of gas hydrates can subsequently plug the oil and gas flowlines, resulting in disruption to production, economic losses, and adverse environmental impacts.^{10–13} Therefore, hydrate inhibitors were developed to treat the hydrate issues with chemicals. Thermodynamic hydrate inhibitors (THIs) and low-dosage hydrate inhibitors (LDHIs), kinetic hydrate inhibitors (KHIs) or antiagglomerants (AAs), are the most commonly used hydrate inhibitors to prevent hydrate or plug formation, respectively.^{14,15} THIs (e.g., methanol and glycol) can prevent hydrate formation by shifting the operating conditions outside of the hydrate stability zone.¹⁶ However, large concentrations (e.g., 30–40 vol %) of THIs are usually required. Therefore, KHIs and AAs classified as LDHIs, typically effective at 0.5–2 vol %, are of significant interest.^{14,17–19} KHIs are used to delay hydrate nucleation and growth times by affecting the hydrogen-bonding network of water.¹⁴ Conversely, AAs work by preventing hydrate particle agglomeration, managing hydrate formation risks, and extending the lifespan of the production assets.^{20–22} The prevention of hydrate particles from agglomeration not only affects flow assurance in oil and gas fields but also other technological applications, such as energy storage (natural gas and hydrogen), gas separation, desalination, and so forth.

AAs, while still allowing hydrate formation in the flowlines, aim to reduce interparticle interactions to prevent agglomeration into large masses. AAs are amphiphilic chemicals with hydrophobic tails and hydrophilic headgroups that can interact with hydrate particle surfaces and make them repulsive/less attractive to other hydrate particles.¹⁸ Most AAs are surface-active molecules and can be adsorbed at water–liquid hydrocarbon or hydrate–liquid hydrocarbon interfaces.²³ Previous studies suggested that the adsorption of AA molecules is one mechanism that may help prevent gas hydrate agglomeration.^{23,24}

The interfacial properties of gas hydrate crystals are critical to dictating how hydrates nucleate/form and interact with each other; all energy applications can be controlled by the interfacial interactions of hydrate crystals in water, liquid hydrocarbon, and gas-continuous systems. In a liquid hydrocarbon-dominated system, a water layer between gas hydrate particles acts to minimize the free energy of the system.²⁵ The addition of chemical additives can significantly alter the interfacial properties of hydrate/water/liquid hydrocarbon systems, such as interfacial tension and contact angle, thereby changing the interparticle and particle-surface forces.^{26,27} Three main mechanisms that can result in particle cohesive force have been proposed: (1) solid–solid interaction between hydrate particles; (2) capillary attraction in which a water bridge connects two hydrate particles; and (3) hydrate sintering.²³ When AA polar headgroups are adsorbed on the gas hydrate surface, the growth rate of gas hydrate could be reduced.²³ Other hypotheses suggest that an AA may reduce the water–liquid hydrocarbon interfacial tension or prevent hydrate growth within the water bridge.^{24,28–30}

To further understand the mechanisms of AAs, recent studies used molecular dynamics (MD) simulations to investigate the particle–surfactant interactions at a molecular level. Phan et al.³¹ investigated the coalescence between one water droplet and one hydrate particle using MD simulation. The study reported that the adsorption of surfactants on both the droplet and the hydrate particle can prevent the water from

adhering to the hydrate surface. Bui and co-workers³² conducted equilibrium MD simulations to study how AA molecules adsorbed at the hydrate–liquid hydrocarbon interface. The study suggested that when the length of long tails in AA molecules is comparable to the length of the liquid hydrocarbon chains in the bulk mixture, the liquid hydrocarbon and AA molecules can yield a densely ordered film that covers the hydrate surface. Another interesting observation from their simulation was that AAs with better performance can yield densely ordered films at the hydrate–liquid hydrocarbon interface, where methane molecules are excluded. Additionally, AAs with long *n*-butyl tails can inhibit the hydrate growth, while the AAs with short *n*-butyl tails may enhance growth by stabilizing the cages near the growing hydrate.¹⁰ Naullage et al.⁷ also used MD simulations to study how the AAs change the wettability of the gas hydrate surface. They suggested that a compact, ordered barrier can only be formed when dodecanal is placed in dodecane mixtures. The study also revealed that the contact angle of a water droplet on the hydrate surface, though significant, may be insufficient to predict the AA performance ability.²⁷ However, these previous studies show that the surfactant-covered hydrate–liquid hydrocarbon interfaces are hydrophobic.^{6,27}

Solid hydrate particles can agglomerate through collisions with other hydrates.^{27,33} Insight into the properties and mechanisms of the agglomeration can be provided by the cohesive forces.^{34,35} From previous studies,^{30,36,37} the capillary liquid bridge (CLB) theory was shown to be the most appropriate model to explain the hydrate particle cohesive force phenomenon. This model describes the liquid bridge

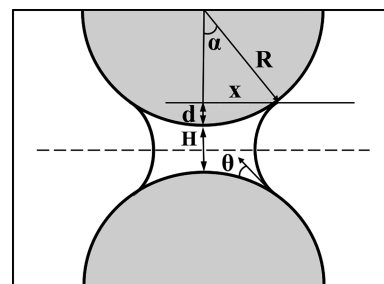


Figure 2. Schematic of the gas hydrate particle–particle interaction with the CLB, where θ is the contact angle between the gas hydrate particle and the liquid bridge, α is the embracing angle, H is the particle separation distance, d is the liquid bridge immersion depth, and R is the radius of a gas hydrate particle.

present between particles (as shown in Figure 2), which is shown in eq 1:

$$F_A = 2\pi\gamma\sin\alpha\sin(\theta + \alpha)R^* + \frac{2\pi\gamma\cos\theta}{1 + \frac{H}{2d}}R^* \quad (1)$$

where F_A is the cohesive force, γ is the interfacial tension between the liquid bridge and the bulk fluid, θ is the contact angle between the gas hydrate particle and the liquid bridge, α is the embracing angle, H is the particle separation distance, d is the liquid bridge immersion depth, and R^* is the harmonic mean radius of two gas hydrate particles.³⁸

Previous experimental studies used an ambient pressure micromechanical force (MMF) apparatus to study the cohesive force (interparticle interaction) between CyC5 hydrate

particles.^{17,26,27} Brown et al. showed potential correlations (in some cases, but not all) between interfacial tension and cohesive force in the presence of chemical additives²⁶ and between cohesive force and contact angle measurements.²⁷ These results agreed with the CLB shown in eq 1. These previous studies suggested that a correlation may be available between the cohesive force and interfacial parameters, such as the contact angle. It is difficult, however, to perform numerous experiments and develop universal correlations that can cover all different scenarios, particularly when the AA molecular structures are not well defined.

Morrissy et al.³⁹ observed that natural surface-active (AA) components can reduce the film growth rate by at least one order of magnitude. These AAs also reduced the cohesive force by 80%.⁴⁰ Li et al. used Span80 as a surfactant in the system and showed that the adsorption of Span80 on the water droplet surface made the interfaces more stable, thus preventing hydrate agglomeration.⁴¹ They also showed that the capillary forces decreased with a higher AA dosage.⁴²

The high-pressure interparticle force device, known as the HP-MMF, was initially described by Brown³⁰ and Lee et al.⁴³ This HP-MMF instrument was used to measure the cohesive forces of ice particles and/or CH₄/C₂H₆ hydrate particles in a gas phase. Wang et al.³³ then performed adhesive force measurements with commercial coatings applied to carbon steel surfaces in a gas phase. The coatings were observed to reduce the interaction between hydrates and surfaces without any corrosion.⁴⁴ The adhesive force of a hydrate particle to an uncoated carbon steel surface (in a gas phase) increased when the carbon steel surface was pre-corroded.³³ In addition, the interparticle cohesive force was observed to decrease with the addition of NaCl. A possible explanation of this cohesive force observation was that the contact angle between hydrate particles and the liquid bridge could have increased.^{33,45}

Hu and Koh⁴⁶ performed the first direct measurement of the CH₄/C₂H₆ gas hydrate cohesive and adhesive force measurements in a model liquid hydrocarbon phase indicating an order of magnitude force increase compared to CyC5 hydrates. It was also observed that the cohesive force between gas hydrates can be increased to greater than 150 mN m⁻¹⁴⁶ after a 12 h shut-in, compared to around 10 mN m⁻¹ for the atmospheric pressure MMF.²⁹ The cohesive force was found to decrease with increasing concentrations of commercial AAs (with unknown structures) in the model liquid hydrocarbon phase. The cohesive force can increase with longer contact time even with commercial AAs present, which can eventually result in a system plugging. This phenomenon could be mitigated when the concentration of the high-performance commercial AA was above 1 vol %, where the cohesive force showed a nonmeasurable value regardless of contact time.⁴⁷ However, in contrast to the current molecular structure AA study, the lack of structure information for previous commercial AA reports made it impossible to relate structure–function properties.

In addition to the cohesive force studies, rocking cells are also applied to investigate the effect of chemical additives on hydrate agglomeration. It was observed that the addition of these chemicals can effectively prevent hydrate particle agglomeration and hence reduce costs in existing systems and future processes.^{48–50} Bui et al.³² confirmed that the test results from a rocking cell are consistent with those from MD simulation. Rocking cell tests were also conducted to compare the performance of different model chemicals,^{12,51–53} inves-

tigate the interactions between hydrates and other flow assurance elements,⁵⁴ and study the effect of synergists^{55,56} and salinities.^{57,58}

While several hypotheses are reported, the structural effect of AAs on determining gas hydrate cohesive force is not fully understood. In this study, an HP-MMF instrument was employed for direct measurements of gas hydrate cohesive force under high-pressure and low-temperature conditions in the presence of AA molecules of known structures dosed into the model liquid hydrocarbon phase. The structural effect on the cohesive force is experimentally revealed. The AAs used in this work have also been tested in industry-standard laboratory rocking cells. Compared to the results at the interfacial level provided by HP-MMF, rocking cells offer the macroscopic-scale evaluation and observation of AAs for their hydrate dispersion performance under specific field conditions. Both apparatuses provide information on the structure of AAs that can effectively reduce gas hydrate agglomeration and show consistent results on the overall performance of the selected AAs.

MATERIALS AND EXPERIMENTAL METHOD

Materials. HP-MMF experiments utilized deionized (DI) water during the water phase and three model liquid hydrocarbons: model liquid hydrocarbon (see Table S1), *n*-dodecane (C₁₂H₂₆, ≥ 99%, Sigma-Aldrich), and *n*-heptane (C₇H₁₆, ≥ 99%, Sigma-Aldrich). The gas mixture used in these experiments comprised 75.7 mol % of methane and 25.3 mol % of ethane provided by Specialty Gases of America Inc. This gas mixture forms sII hydrate,^{59,60} which typically forms in oil and gas flowlines.

The rocking cell tests used the Green Canyon gas mixture (the composition is shown in Table 1) and two model liquid hydro-

Table 1. Composition of the Natural Gas Mixture Used in the Rocking Cell.

composition	mol %
N ₂	0.39
<i>n</i> -C1	87.26
<i>n</i> -C2	7.57
<i>n</i> -C3	3.10
<i>i</i> -C4	0.49
<i>n</i> -C4	0.79
<i>i</i> -C5	0.20
<i>n</i> -C5	0.20

carbons: *n*-dodecane (C₁₂H₂₆, ≥ 99%, Sigma-Aldrich) and *n*-octane (C₈H₁₈, ≥ 99%, Sigma-Aldrich). Quaternary ammonium surfactants are widely used as AAs in the gas hydrate systems.^{12,14} Therefore, four quaternary ammonium surfactant molecules are used as AAs in this study (provided by Multi-Chem, a Halliburton service). Figure 3 shows their structures. For simplicity, they are named as follows: (a) AA-C8; (b) AA-C12; (c) AA-C18–1; and (d) AA-C18–2. The main difference between AA-C8 and AA-C12 is their tail lengths. For AA-C18–1 and AA-C18–2, the major differences are the number of double bonds between two carbon atoms.

EXPERIMENTAL METHOD

HP-MMF. Figure 4 shows the schematic of the HP-MMF system, including the testing section, aluminum cell, stirrer and stir bar (VWR Model 230), feedthroughs, nanomanipulator (manufactured by Klocke Nanotechnik), pressure transducer (OMEGA, PX309-3KGSV, BSL accuracy of ±0.08%), and thermocouple (OMEGA, TMQSS-032G-6, uncertainty consisting of >1 K or 0.75%). The testing section was made of stainless steel to sustain pressures of up to 10.3 MPa; therefore, a broad spectrum of gas hydrate formers and

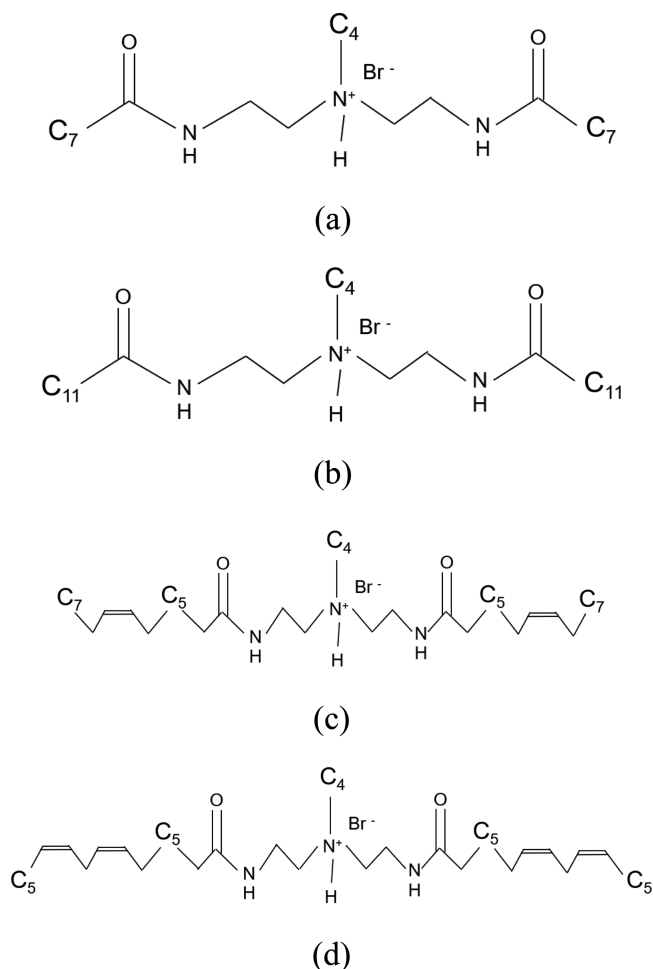


Figure 3. Detailed structures of the four AAs used in this study: (a) AA-C8; (b) AA-C12; (c) AA-C18-1; and (d) AA-C18-2.

conditions can be applied and studied. Based on this apparatus, gas hydrate cohesive force measurements were performed between two gas hydrate particles in model liquid hydrocarbon using the HP-MMF. Further details of the experimental procedure of gas hydrate cohesive force measurements in the presence of AAs are available in a previous publication.⁴⁶

Rocking Cell. A system of advanced high-pressure rocking cells at Multi-Chem, a Halliburton service was used to test the performance of the AA molecules⁶¹ at the macroscopic scale. Rocking cells are primarily used to analyze and evaluate the performance of AAs. The system enables the possibility to test the transportability of the

dispersed gas hydrate particles under fluid flow. The cells feature dual sapphire windows and a powerful LED lighting system that allows for the clear observation of oilfield fluids under hydrate conditions. The dual-window design also features a center-ported transducer and gas supply connections that eliminate issues with fluids contaminating the connecting tubing and hydrating up. The design generates more reliable and accurate pressure data. Each cell consists of a Hastelloy cylindrical body of 4.5 inches in length and 0.7 inches in diameter. The cell also houses two proximity sensors that detect and record any obstruction in the movement of the metal sphere that is placed in each cell for agitation. More details of the rocking cell system can be found from previous publications.^{62,63}

The system can be program-controlled to set temperatures, temperature ramp rates, rocking rates, and rocking angles. Both shut-in and restart scenarios can be simulated to mimic the flowline operations. The shut-in period is performed by stopping the rocking of the cell while maintaining a constant temperature. When the cells are restarted to rock again, the restart period begins. The system is rated up to 20 MPa and can be temperature controlled from 248 to 343 K via a glycol cooling bath. The pressure sensor has an accuracy of 0.01 MPa, and temperature can be measured within ± 0.1 K.

Figure 5 shows a close-up photograph of the rocking cell rigs.

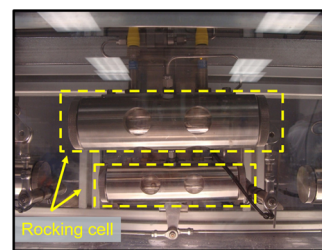


Figure 5. Close-up of a six-unit rocking cell rig with optical viewing ports. Gas, liquid hydrocarbon, and water (or brine) are injected into the cell before the test.⁶¹

The required amounts of liquid hydrocarbon, water, and inhibitor were injected into the cells. In these experiments, *n*-dodecane or *n*-octane was used as the liquid hydrocarbon phase, and 3.5 wt % NaCl brine was used as the aqueous phase. Thereafter, the cells were pressurized to 13.8 MPa with a natural gas mixture, a common Gulf of Mexico Type II hydrate former. Testing was conducted at constant volume after the initial saturation phase, and no additional gas was added during the cooldown phase and thereafter.

After pressurizing the cells, a 2 h saturation period for liquid hydrocarbon was followed by a 1 h cooldown period, where the temperature was ramped down from 293 to 277 K. After reaching the designated temperature, the cells were then rocked for 16 to 18 h and shut-in horizontally for 6 h. The cells were then restarted for 0.5 h,

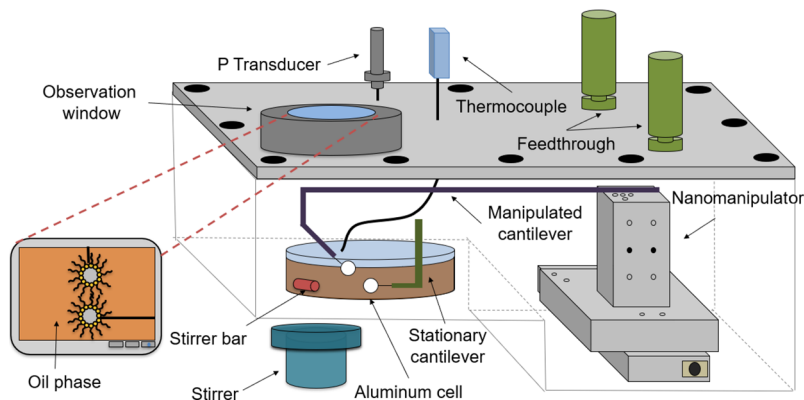


Figure 4. Schematic of the HP-MMF experimental setup (reprinted with permission from Hu and Koh⁴⁶).

and particular attention was given to the critical restart period. Finally, the cells were warmed back to 293 K while rocking. These tests were conducted to simulate steady-state as well as transient conditions in the field. The AA, after injection at the wellhead, would flow along with the production fluids, and a subsequent shut-in would occur in the field. This would be followed by a restart.

RESULTS AND DISCUSSION

The addition of AAs is commonly required during oil and gas production in flowlines and transportation through umbilical lines. AAs can alter the interfacial properties thereby changing the gas hydrate interparticle interactions. As discussed previously, the cohesive force can be used as a parameter to determine the performance of AAs.³³ In this section, the cohesive forces in the presence of four AA molecules and two liquid hydrocarbons, *n*-dodecane (C₁₂H₂₆) and *n*-heptane (C₇H₁₆), are presented. The effect of salinity is also reported in this study. Finally, rocking cell tests show qualitative agreement with HP-MMF results on the performance of AAs.

Cohesive Force between Gas Hydrate Particles.

Cohesive force experiments were performed at 3.45 MPa and 274 K with different AAs in the presence of *n*-dodecane or *n*-heptane. The subcooling is estimated (using CSMGem⁴⁹) at 9.4 K throughout the entire cohesive force study. In addition to 10 s contact between gas hydrate particles, this study also shows the interparticle cohesive force when the contact time is 10 min to simulate the shut-in process in oil and gas flowlines. A 0–7.5 wt % salinity is applied for AA-C8 and AA-C12.

Prior studies showed that 0.5 vol % high-performance commercial AA was able to reduce the cohesive force to $0.9 \pm 0.3 \text{ mN m}^{-1}$ from $23.5 \pm 2.5 \text{ mN m}^{-1}$ (baseline) in a model liquid hydrocarbon. A low-performance commercial AA resulted in a higher cohesive force of $3.9 \pm 0.9 \text{ mN m}^{-1}$, even when the concentration was increased to 1 vol %. The structures of the commercial AAs were all unknown in previous work.⁴⁷ In comparison, cohesive force measurements of AAs with known molecular structures are shown in Figure 6. Compared to the baseline test results without any AAs ($23.5 \pm 2.5 \text{ mN m}^{-1}$), all four AAs can decrease the cohesive force between gas hydrate particles. However, when the liquid hydrocarbon phase changes from *n*-dodecane to *n*-heptane, the

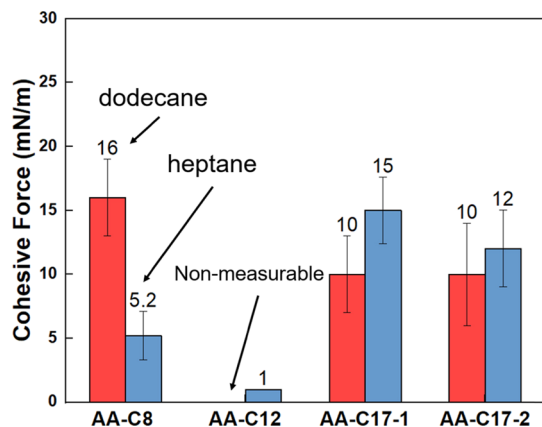


Figure 6. Cohesive force measurements in systems with the four AAs at contact times of 10 s and concentration of 0.5 vol %: *n*-dodecane, red; *n*-heptane, blue. Gas hydrates were formed using a CH₄/C₂H₆ gas mixture at 3.45 MPa and 274 K in *n*-dodecane or *n*-heptane. Each bar represents at least 40 pull-offs for two or more particle pairs. Error bars represent the 95% confidence interval of a *t*-distribution.

cohesive force values change. For example, the cohesive force reduces from 16 ± 3.2 to $5.2 \pm 1.9 \text{ mN m}^{-1}$ when the liquid hydrocarbon phase changes from *n*-dodecane to *n*-heptane for AA-C8, while other operating conditions (e.g., pressure, temperature, annealing time, contact time, etc.) remain the same. Compared to AA-C8, AA-C12 shows lower cohesive force regardless of the liquid hydrocarbon phase, hence indicating higher antiagglomeration behavior.

In this study, the variations observed in cohesive force with different liquid hydrocarbon phases can be explained by the change in the antiagglomeration molecular effect of the AAs. With the knowledge of the AA structures, AA-C8 has eight carbon alkanes on long tails, which is closer to the chain length of *n*-heptane compared to *n*-dodecane. When the long tails of AA molecules have a similar length to the liquid hydrocarbon chains, the AA molecules may form a densely ordered thin film that can prevent water molecules from penetrating the gas hydrate surface, yielding a low particle interaction.³² This hypothesis is also supported by the experiments with the other three AAs shown in Figure 6. AA-C12 shows a slightly higher cohesive force in *n*-heptane compared to the nonmeasurable force in *n*-dodecane because 12 carbon atoms in the AA tails are closer to the length of *n*-dodecane. AA-C17-1 and AA-C17-2 also show higher cohesive forces in *n*-heptane compared to *n*-dodecane because the chain lengths of these AAs are closer to the length of *n*-dodecane compared to *n*-heptane.

The addition of surfactants into the system can lead to a reduction of liquid hydrocarbon–water and/or hydrate–liquid hydrocarbon interfacial tensions and can change the hydrate surface wettability by increasing the contact angle of a water droplet on the gas hydrate surface.^{27,64–66} To study these effects, the interfacial tensiometer (IFT) was used to perform the pendant drop interfacial tension measurements. Because of the addition of AAs, all IFT values were obtained after the tests reached equilibrium, indicating the completion of the surfactant adsorption on the liquid hydrocarbon–water interface. Figure 7 shows the IFT results for the four AAs in

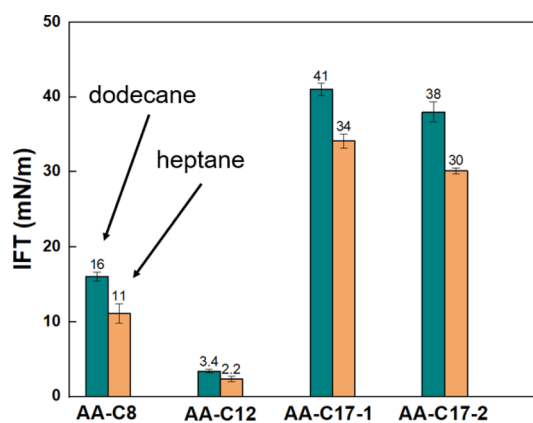


Figure 7. Interfacial tension measurements using the four AAs in *n*-dodecane and *n*-heptane.

both *n*-dodecane and *n*-heptane. The IFT for AA-C12 is significantly lower compared to other AAs, which may lead to a low cohesive force from eq 1, if other parameters remain constant. However, the results for the other three AAs are not consistent with the cohesive force results as indicated in Figure 6. This inconsistency between the cohesive force and liquid

hydrocarbon–water IFT is also observed in previous publications, indicating that the liquid hydrocarbon–water interfacial tension is insufficient to predict the performance of AAs.^{17,29}

According to the capillary bridge eq 1, when the contact angle of a water droplet on the hydrate surface is obtained, the measured cohesive force and the interfacial tension can be used to estimate the curvature of the liquid bridge, which is described by the embracing angle, α and the particle separation distance, H . Previous studies showed the contact angle measurements in the presence of AAs. The contact angle was measured to be 180° when a high-performance AA was present in the system, whereas the contact angle reduced to around 88° when a low-performance AA was added.²⁴ Based on the cohesive force values, AA-C12 can be classified as a high-performance AA and the other three AAs are classified as low-performance AAs. When the cohesive force, interfacial tension for AA-C12, and the contact angle for a high-performance AA are used in eq 1, the estimated embracing angle could be smaller than 0.05° and the separation distance is greater than $1\ \mu\text{m}$, indicating that the water bridge is narrow and the two hydrate particles are relatively far from each other. However, if the cohesive forces and the interfacial tensions for the other three AAs and the contact angle for a low-performance AA are applied in eq 1, the embracing angle increases by two orders of magnitude to 2° and the separation distance can be smaller than $500\ \text{nm}$, resulting in a wider and thinner water bridge. The latter result indicates that when a low-performance AA is added, the contact area between the hydrate surface and the water bridge increases, and the separation distance, or the thickness of the water bridge, can be reduced. Conversely, a high-performance AA aims to minimize the hydrate contact to the water bridge and maximize the distance between two hydrate particles to effectively reduce the interactions between hydrate particles.

It has been proposed from previous MD simulations that the similarity of chain lengths in surfactant AA molecules and liquid hydrocarbons is essential to form an aligned film at the hydrate–liquid hydrocarbon interface.³² However, these experimental results reported for AA-C8 and AA-C12 are inconsistent in part with the prior work:³² AA-C12 has a much lower cohesive force in *n*-heptane compared to AA-C8 in *n*-heptane, although the tail length of AA-C8 is much closer to the length of *n*-heptane. This inconsistency can be explained by the travel distance (the thickness of the barrier that is formed by the AA molecules) of the water penetration (Figure 8) and the destabilization of the water bridge (Figure 9). Assuming that the number of AA molecules is the same on the hydrate–liquid hydrocarbon interface, AA-C12 has a much longer alkyl tail compared to AA-C8, which can lead to a thicker film on

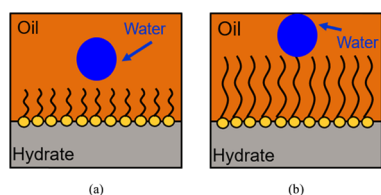


Figure 8. Conceptual illustration of the water molecule penetrating the thin film of AA molecules formed by: (a) AA-C8 and (b) AA-C12 on the hydrate–liquid hydrocarbon interface. The sizes of the water and AA molecules are exaggerated to improve visualization.

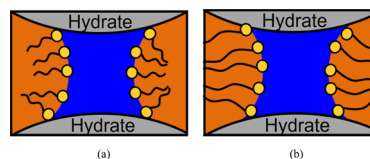


Figure 9. Conceptual illustration of how (a) AA-C8 and (b) AA-C12 molecules could destabilize the water bridge between two gas hydrate particles. The sizes of the water and AA molecules are exaggerated to improve visualization.

the hydrate surface. When water molecules attempt to approach the hydrate–liquid hydrocarbon interface, the thicker barrier of the AA molecules can significantly increase the travel distance and time for the water molecules to the hydrate surface, leading to a reduction on the cohesive force between gas hydrate particles.⁶ AAs can bind not only to the hydrate–liquid hydrocarbon interface^{30,67} but also to the hydrate–water interface.^{68,69} Figure 9 shows that the AAs may be able to destabilize the water bridge between gas hydrate particles by disrupting water molecules in the water bridge. The capability of the destabilization depends on the length of the hydrophobic group (alkyl tail) of the AA molecules. AA-C12 has a stronger interaction with *n*-dodecane compared to the AA-C8 with the same liquid hydrocarbon, if the binding between the hydrophilic head and the water molecules is the same for both AAs. Therefore, it is easier for AA-C12 to disrupt or drag the water molecules toward the liquid hydrocarbon phase compared to AA-C8, leading to a stronger destabilization effect on gas hydrate cohesion.

However, lower cohesive force of AA-C12 compared to AA-C8 also indicates that it may not be possible to form an ordered dense barrier for short-chain AAs in short-chain liquid hydrocarbons. Previous MD simulations have reported that even high concentrations of short alkyl chain surfactants do not result in the formation of a compact monolayer at the hydrate surface. They showed that both pure and mixed hexanol–hexane monolayers are not ordered and not densely formed.^{6,32} Therefore, the compatibility of the length of AAs and liquid hydrocarbons is not the only indicator to ensure the formation of a compact, ordered AA film on the hydrate surface or to evaluate the performance of AAs. The compact barrier has more opportunities to be formed with longer-tail AA molecules in longer-chain liquid hydrocarbons. The observations in this study are in agreement with MD simulation results in prior work.⁷⁰

Effect of NaCl. It is known that salt can inhibit hydrate formation and shift the hydrate equilibrium conditions,^{1,71–75} thereby affecting the performance of AAs.^{76–80} To further investigate the effect of salt (NaCl in this study) on the gas hydrate surfaces and interparticle interactions, experiments were conducted at constant subcooling, which provides the same driving force to form hydrates with and without NaCl. Figure 10 shows the cohesive force measurements in the systems with the AA-C8 and AA-C12 at 0, 3.5, 5, and 7.5 wt % of NaCl in DI water. It was observed that the cohesive force between gas hydrate particles was reduced with salinity. When the salinity increased to 7.5 wt %, the cohesive force decreased from $16 \pm 3.2\ \text{mN m}^{-1}$ to being nonmeasurable for 0.5 vol % AA-C8, indicating that NaCl is capable of promoting AA molecular performance at constant subcooling. However, AA-C12 showed different behavior. Cohesive force with AA-C12 remained nonmeasurable regardless of the salinities, indicating

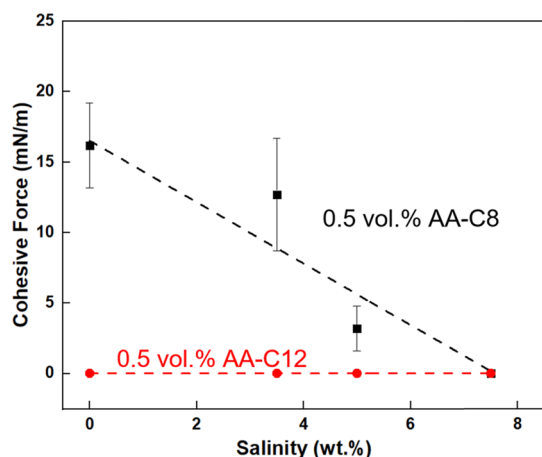


Figure 10. Cohesive force measurements in systems with the AA-C8 (black) and AA-C12 (red) at salinities ranging from 0 to 7.5 wt %. Gas hydrates were formed using a $\text{CH}_4/\text{C}_2\text{H}_6$ gas mixture at 3.45 MPa and 274 K in *n*-dodecane. Each data point represents at least 40 pull-offs. Error bars represent the 95% confidence interval of a *t*-distribution.

no salt concentration dependence (at least for the AA concentrations measured). As previously discussed, AA-C12 showed a nonmeasurable force when no NaCl was present in the system, leading to superior performance compared to other AAs. AA-C12 provides the same high performance at various salinities.

Previous studies reported that the addition of salt in water can lead to a reduction of the interfacial tension (when the salinity is lower than 10 wt %) because the Na^+ and Cl^- ions can interact with water molecules.^{65,81,82} When AAs are present in the system, Na^+ and Cl^- ions can be hydrated on the AA and water molecules, thereby reducing the interaction between AA and water molecules, resulting in a reduction in the liquid hydrocarbon–water interfacial tension.^{81,82}

The addition of salt should not lead to a different conversion of hydrate or unconverted water²⁹ on the hydrate surfaces because of the constant subcooling during each experiment. The reason that NaCl can promote the performance of AAs may be explained by the surface roughness of gas hydrate particles. It has been proposed that the addition of NaCl in the formation of hydrate can lead to rougher hydrate surfaces. To test this hypothesis, here we examine the surface of gas hydrate particles by visually observing them through the microscope. Figure 11 presents the gas hydrate particle surfaces with (a) 0 wt %; (c) 7.5 wt % salinity immediately after the completion of the hydrate formation process. It is obvious that the hydrate formed using DI water shows a much smoother surface compared to the hydrate formed with 7.5 wt % brine. A previous study by Vetráková et al. revealed that the amount of salt precipitated on the ice surface is increasing with higher salinity. Similarly, with more salt present the hydrate surface roughness may increase.⁸³ The higher roughness of the gas hydrate surface may lead to a reduction of the contact area between two solid particles, eventually resulting in a reduction on cohesive force. Therefore, the addition of NaCl may increase the surface roughness of gas hydrates and finally lead to lower cohesive force between gas hydrate particles.

To test the effect of the contact/shut-in period, experiments at various salinities were also performed at a contact time of 10 min compared to 10 s (this timescale is significant for this

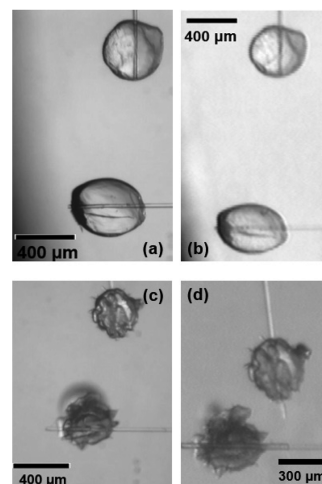


Figure 11. Gas hydrate particles formed using 0.5 vol % AA-C8 with (a) 0 wt % salinity at 10s contact time; (b) 0 wt % salinity at 10 min contact time; (c) 7.5 wt % salinity at 10s contact time; and (d) 7.5 wt % salinity at 10 min contact time; experiments used a $\text{CH}_4/\text{C}_2\text{H}_6$ gas mixture at 3.45 MPa and 274 K in *n*-dodecane.

experimental scale). Previous studies reported cohesive force tests from 10 s to 24 h. contact time. Higher cohesive force was observed with longer contact time in a model liquid hydrocarbon phase without AAs and salt. After 18 h contact, the cohesive force increased to greater than 150 mN m⁻¹. When commercial AAs (with unknown structures) were introduced to the system, the cohesive force decreased compared to the system without AA at the same contact time. However, when AAs are under-dosed in the system, the cohesive force increased with the contact time.^{46,47} Figure 12

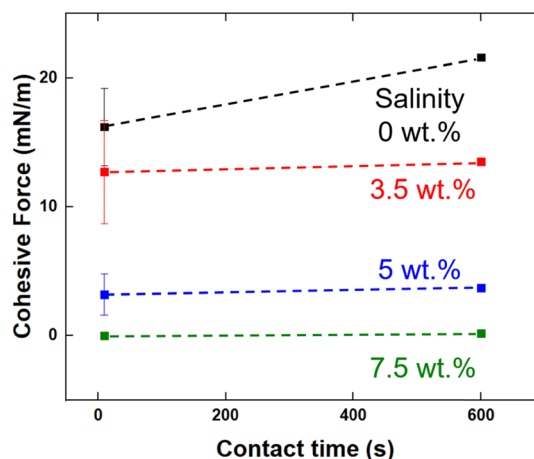


Figure 12. Cohesive force measurements in systems with the AA-C8 at salinity from 0 to 7.5 wt % and contact time of 10s and 10 min. Gas hydrates were formed using a $\text{CH}_4/\text{C}_2\text{H}_6$ gas mixture at 3.45 MPa and 274 K in *n*-dodecane. Each data point at 10 s contact represents at least 40 pull-offs. Error bars represent the 95% confidence interval of a *t*-distribution.

shows the cohesive force measurements at 0, 3.5, 5, and 7.5 wt % salinity using contact times of 10 s and 10 min. A 0.5 vol % AA-C8 is applied throughout this entire part of the study. It was observed that the cohesive force increased from 16 ± 3.2 to 22 mN m^{-1} (cohesive force measurement at 10 min contact time was performed once because of the long contact period)

as the contact time increases. However, when the salinity increases from 0 to 7.5 wt %, the effect of contact time is gradually eliminated, leading to nonmeasurable forces for 7.5 wt % NaCl regardless of contact time. It should be noted that the change in hydrate particle morphology during the contact time period from 10s to 10 min is negligible when the salinity remains constant (as shown in Figure 11a,b for 0% salinity and c,d for 7.5 wt % salinity). Even though the performance of AA-C8 is lower than that of AA-C12 at 0 wt % salinity, the higher salinity promotes the performance of AA-C8 and eventually leads to nonmeasurable forces at various contact times. This observation demonstrated that the addition of NaCl can further enhance the effect of AAs.

Rocking Cell Tests of AA Molecule Performance in Different Liquid Hydrocarbons. To test the reliability of the results from HP-MMF, industry-standard rocking cell tests were performed. During these tests, AA typical dosing was based on the total amount of water present in the system. Hydrate agglomeration and plugging tendency increase with increasing the total amount of water. To determine the amount of water present in the system, watercut (the volume of water with respect to the total volume of liquid in the system) is generally used.^{84,85} Each of the four AAs was directly applied in the rocking cell system to evaluate the performance. Rocking cell experiments were conducted at constant volume and water volume percentage under fluid shear. It should be noted that the rocking cell experiments are performed with 30 vol % water, whereas the HP-MMF experiment was conducted at 10 vol % watercut (because of the water volume percentage limitation of the HP-MMF).

The performance of AAs was evaluated both quantitatively and qualitatively. Quantitatively, the viscosity of the testing fluid under pressure at 277 K should allow for a magnetic ball to travel from one end of the cell to the other. In addition, besides viscosity, observations of the testing fluid throughout the test (i.e., during cooldown, after cooldown, before shut-in, after shut-in, and restart) were highly crucial. Any notable hydrate particle agglomeration, deposition onto the walls of the sapphire tube, or settling of agglomerates at the bottom of the tubes would constitute a “fail” in the rocking cell test.

Table 2 summarizes the experimental data obtained using the four AAs with *n*-dodecane or *n*-octane (C₈H₁₈). It is worth noting that although *n*-heptane was used in the HP-MMF instead of *n*-octane, the alkane chain length of *n*-heptane is only shorter by one carbon atom. Therefore, the effect of the alkane chain length should be insignificant in terms of AA performance. From the experimental results, AA-C12 main-

tains ultrafine hydrate particles and a fully flowable system (graded as a “pass” in Table 2) for both *n*-dodecane and *n*-octane, while other AAs are evaluated as failures (system plugs with visible deposits and a stuck ball) for either liquid hydrocarbon. These results are in qualitative agreement with the HP-MMF experiments, where the AA-C12 shows superior performance compared to the other three AAs in both liquid hydrocarbons. Table 2 illustrates that the grading criterion is 5 for AA-C12 in *n*-dodecane and 4 for AA-C8 in *n*-octane. This interesting observation is quantitatively consistent and strongly supported by the data shown in Figure 6, where the nonmeasurable cohesive force was obtained for AA-C12 in *n*-dodecane and slightly increased (1 mN m⁻¹) for AA-C12 in *n*-octane.

CONCLUSIONS

This study provides insights into gas hydrate interparticle interactions at both interfacial and macroscopic levels using HP-MMF and industry rocking cells. We observed that the AA-C12 molecule has superior performance compared to other AA molecules in both *n*-dodecane and *n*-heptane by evaluating the cohesive force. It was experimentally suggested that the AA molecule with a longer alkyl chain length can lead to a thicker barrier, and the AA molecules may have higher packing density when the AA alkyl tail length is comparable to that of the liquid hydrocarbon chain on the gas hydrate surfaces. The superior performance of AA-C12 in both liquid hydrocarbons could be explained by the reduction of water penetration and the destabilization of the water bridge. NaCl was observed to promote the performance of AA-C8, whereas AA-C12 gives nonmeasurable force regardless of salinity (at the AA concentrations tested). Increasing salinity can also eliminate the effect of contact and shut-in time. This work provides investigations of the structural effect on the known molecular structure AAs. The results show that these molecules are able to reduce the interfacial tension and increase the gas hydrate–water contact angle, thereby minimizing the gas hydrate interparticle interactions. In addition, the combination of HP-MMF and rocking cell results reveals similar behaviors when evaluating the performance of AAs, although the experimental conditions are different. These results also show that the experiments at the interfacial scale (HP-MMF) can be transferred to macroscopic-scale apparatuses, such as rocking cells. The combination of HP-MMF and rocking cell evaluations reveals similar behavior and trends when evaluating the length effect of AA tails compared to that of solvent. Both apparatuses show agreement on the overall performance of the AA molecules, although the experimental conditions are slightly different. The structure–performance relation reported in this work can be used to help improve understanding of the molecular mechanisms and properties of AAs. Understanding the AA structure is a critical step to developing improved AAs for preventing hydrate particle agglomeration and ultimate plug formation. The results reported in this work can help in advancing new AA chemistry for flow assurance strategies of maintaining slurry flow. Future work could study the interaction intensity between salt and AA molecules by utilizing ion chromatography analysis, where the ions can be hydrated differently at various salinities.⁷⁸ The presence of AAs may alter the capillary pressure and hydrate surface wettability.⁸⁶ Therefore, the direct relationship between the capillary pressure and the cohesive force would be also interesting for future studies in the presence of AAs.

Table 2. Summary of the Results of the Four AAs with Variations in Alkyl Tail Lengths in *n*-Dodecane or Octane as the Liquid Hydrocarbon Phase: 3.5 wt % Salinity, 2 vol % Dosage of AAs, and 30 vol % Watercut.

AAs	liquid hydrocarbon	rocking cell (pass/fail)	cohesive force (mN m ⁻¹)
AA-C12	<i>n</i> -dodecane	pass	1 ± 0.1
	<i>n</i> -octane	pass	N/A
AA-C8	<i>n</i> -dodecane	fail	5.2 ± 1.9
	<i>n</i> -octane	fail	N/A
AA-C18–1	<i>n</i> -dodecane	fail	15 ± 2.6
	<i>n</i> -octane	fail	N/A
AA-C18–2	<i>n</i> -dodecane	fail	12 ± 3.0
	<i>n</i> -octane	fail	N/A

■ ASSOCIATED CONTENT

SI Supporting Information

The Supporting Information is available free of charge at <https://pubs.acs.org/doi/10.1021/acs.langmuir.0c02503>.

Composition of the model liquid hydrocarbon (PDF)

■ AUTHOR INFORMATION

Corresponding Author

Carolyn A. Koh – Center for Hydrate Research, Chemical & Biological Engineering Department, Colorado School of Mines, Golden, Colorado 80401, United States; orcid.org/0000-0003-3452-4032; Email: ckoh@mines.edu

Authors

Sijia Hu – Center for Hydrate Research, Chemical & Biological Engineering Department, Colorado School of Mines, Golden, Colorado 80401, United States; Halliburton, Houston, Texas 77032, United States

Loan Vo – Halliburton, Houston, Texas 77032, United States

Deepak Monteiro – Halliburton, Houston, Texas 77032, United States

Scot Bodnar – Halliburton, Houston, Texas 77032, United States

Philippe Prince – Halliburton, Houston, Texas 77032, United States

Complete contact information is available at:

<https://pubs.acs.org/doi/10.1021/acs.langmuir.0c02503>

Notes

The authors declare no competing financial interest.

■ ACKNOWLEDGMENTS

The authors thank Multi-Chem, a Halliburton service for supplying the AA molecules with detailed structures. We also acknowledge the support from the National Science Foundation CBET 2015201.

■ REFERENCES

- (1) Sloan, Jr, E. D.; Koh, C., *Clathrate hydrates of natural gases* 3rd edition ed.; CRC press, Taylor & Francis Group: Boca Raton, FL, 2007.
- (2) Fleischer, E. B.; Janda, K. C. Prediction of Clathrate Structure Type and Guest Position by Molecular Mechanics. *J. Phys. Chem. A* **2013**, *117*, 4001–4010.
- (3) Lo, C.; Zhang, J. S.; Somasundaran, P.; Lu, S.; Couzis, A.; Lee, J. W. Adsorption of Surfactants on Two Different Hydrates. *Langmuir* **2008**, *24*, 12723–12726.
- (4) Zhang, J. S.; Lee, S.; Lee, J. W. Kinetics of Methane Hydrate Formation from SDS Solution. *Ind. Eng. Chem. Res.* **2007**, *46*, 6353–6359.
- (5) Hu, Y.; Lee, B. R.; Sum, A. K. Insight into increased stability of methane hydrates at high pressure from phase equilibrium data and molecular structure. *Fluid Phase Equilib.* **2017**, *450*, 24–29.
- (6) Naullage, P. M.; Bertolazzo, A. A.; Molinero, V. How Do Surfactants Control the Agglomeration of Clathrate Hydrates? *ACS Cent. Sci.* **2019**, *5*, 428–439.
- (7) Kvenvolden, K. A. Gas hydrates—geological perspective and global change. *Rev. Geophys.* **1993**, *31*, 173–187.
- (8) Milkov, A. V. Global estimates of hydrate-bound gas in marine sediments: how much is really out there? *Earth-Sci. Rev.* **2004**, *66*, 183–197.
- (9) Li, Y.; Chen, M.; Liu, C.; Song, H.; Yuan, P.; Zhang, B.; Liu, D.; Du, P. Effects of Layer-Charge Distribution of 2:1 Clay Minerals on

Methane Hydrate Formation: A Molecular Dynamics Simulation Study. *Langmuir* **2020**, *36*, 3323–3335.

(10) Bui, T.; Sicard, F.; Monteiro, D.; Lan, Q.; Ceglie, M.; Burrese, C.; Striolo, A. Antiagglomerants Affect Gas Hydrate Growth. *J. Phys. Chem. Lett.* **2018**, *9*, 3491–3496.

(11) Mitarai, M.; Kishimoto, M.; Suh, D.; Ohmura, R. Surfactant Effects on the Crystal Growth of Clathrate Hydrate at the Interface of Water and Hydrophobic-Guest Liquid. *Crystal Growth Design* **2015**, *15*, 812–821.

(12) Chua, P. C.; Kelland, M. A. Study of the Gas Hydrate Anti-agglomerant Performance of a Series of n-Alkyl-tri(n-butyl)-ammonium Bromides. *Energy Fuels* **2013**, *27*, 1285–1292.

(13) Hammerschmidt, E. G. Formation of Gas Hydrates in Natural Gas Transmission Lines. *Ind. Eng. Chem.* **1934**, *26*, 851–855.

(14) Kelland, M. A. History of the Development of Low Dosage Hydrate Inhibitors. *Energy Fuels* **2006**, *20*, 825–847.

(15) Kelland, M. A., *Production Chemicals for the Oil and Gas Industry*. CRC Press: 2009.

(16) Hu, Y.; Makogon, T. Y.; Karanjkar, P.; Lee, K.-H.; Lee, B. R.; Sum, A. K. Gas Hydrates Phase Equilibria and Formation from High Concentration NaCl Brines up to 200 MPa. *J. Chem. Eng. Data* **2017**, *62*, 1910–1918.

(17) Aman, Z. M.; Olcott, K.; Pfeiffer, K.; Sloan, E. D.; Sum, A. K.; Koh, C. A. Surfactant Adsorption and Interfacial Tension Investigations on Cyclopentane Hydrate. *Langmuir* **2013**, *29*, 2676–2682.

(18) Perrin, A.; Musa, O. M.; Steed, J. W. The chemistry of low dosage clathrate hydrate inhibitors. *Chem. Soc. Rev.* **2013**, *42*, 1996–2015.

(19) Lederhos, J. P.; Long, J. P.; Sum, A.; Christiansen, R. L.; Sloan, E. D. Effective kinetic inhibitors for natural gas hydrates. *Chem. Eng. Sci.* **1996**, *51*, 1221–1229.

(20) Rogers, R., Hydrate Inhibition During Drilling and Production. In *Offshore Gas Hydrates*, Rogers, R., Ed. Gulf Professional Publishing: Boston, 2015; 151–187.

(21) Sloan, E. D. Gas Hydrates: Review of Physical/Chemical Properties. *Energy Fuels* **1998**, *12*, 191–196.

(22) Mao, W. L.; Mao, H.-K. Hydrogen storage in molecular compounds. *Proc. Natl. Acad. Sci. U. S. A.* **2004**, *101*, 708–710.

(23) Kelland, M. A.; Svartås, T. M.; Andersen, L. D. Gas hydrate anti-agglomerant properties of polypropoxylates and some other demulsifiers. *J. Petrol. Sci. Eng.* **2009**, *64*, 1–10.

(24) Kelland, M. A.; Svartaas, T. M.; Øvsthus, J.; Tomita, T.; Mizuta, K. Studies on some alkylamide surfactant gas hydrate anti-agglomerants. *Chem. Eng. Sci.* **2006**, *61*, 4290–4298.

(25) Aman, Z. M.; Koh, C. A. Interfacial phenomena in gas hydrate systems. *Chem. Soc. Rev.* **2016**, *45*, 1678–1690.

(26) Brown, E. P.; Koh, C. A. Competitive Interfacial Effects of Surfactant Chemicals on Clathrate Hydrate Particle Cohesion. *Energy Fuels* **2016**, *30*, 8065–8071.

(27) Brown, E. P.; Hu, S.; Wells, J.; Wang, X.; Koh, C. A. Direct Measurements of Contact Angles on Cyclopentane Hydrates. *Energy Fuels* **2018**, *32*, 6619–6626.

(28) Huo, Z.; Freer, E.; Lamar, M.; Sannigrahi, B.; Knauss, D. M.; Sloan, E. D. Hydrate plug prevention by anti-agglomeration. *Chem. Eng. Sci.* **2001**, *56*, 4979–4991.

(29) Aman, Z. M. *Interparticle Phenomena of Cyclopentane Hydrate*. Colorado School of Mines, Golden, CO, 2013.

(30) Brown, E. *Studies of Hydrate Cohesion, Adhesion And Interfacial Properties using Micromechanical Force Measurements*. Ph.D. Thesis, Colorado School of Mines, Golden, CO, 2016.

(31) Phan, A.; Bui, T.; Acosta, E.; Krishnamurthy, P.; Striolo, A. Molecular mechanisms responsible for hydrate anti-agglomerant performance. *Phys. Chem. Chem. Phys.* **2016**, *18*, 24859–24871.

(32) Bui, T.; Phan, A.; Monteiro, D.; Lan, Q.; Ceglie, M.; Acosta, E.; Krishnamurthy, P.; Striolo, A. Evidence of Structure-Performance Relation for Surfactants Used as Antiagglomerants for Hydrate Management. *Langmuir* **2017**, *33*, 2263–2274.

(33) Wang, S.; Hu, S.; Brown, E. P.; Nakatsuka, M. A.; Zhao, J.; Yang, M.; Song, Y.; Koh, C. A. High pressure micromechanical force

measurements of the effects of surface corrosion and salinity on CH₄/C₂H₆ hydrate particle–surface interactions. *Phys. Chem. Chem. Phys.* **2017**, *19*, 13307–13315.

(34) Israelachvili, J. N., *Intermolecular and Surface Forces*. 2nd edition; Great Britain, 1991.

(35) Wang, W.; Li, Y.; Liu, H.; Zhao, P. Study of Agglomeration Characteristics of Hydrate Particles in Oil/Gas Pipelines. *Adv. Mech. Eng.* **2014**, *7*, No. 457050.

(36) Dieker, E. L., *Cyclopentane Hydrate Interparticle Adhesion Force Measurements*. Colorado School of Mines, Golden, CO, 2009.

(37) Taylor, C. J. *Adhesion force between hydrate particles and macroscopic investigation of hydrate film growth at the hydrocarbon/water interface*. Master Thesis, Colorado School of Mines, Golden, CO, 2006.

(38) Aman, Z. M.; Brown, E. P.; Sloan, E. D.; Sum, A. K.; Koh, C. A. Interfacial mechanisms governing cyclopentane clathrate hydrate adhesion/cohesion. *Phys. Chem. Chem. Phys.* **2011**, *13*, 19796–19806.

(39) Morrissy, S. A.; McKenzie, A. J.; Graham, B. F.; Johns, M. L.; May, E. F.; Aman, Z. M. Reduction of Clathrate Hydrate Film Growth Rate by Naturally Occurring Surface Active Components. *Energy Fuels* **2017**, *31*, 5798–5805.

(40) Morrissy, S. A.; Kuteyi, T. O.; Johns, M. L.; May, E. F.; Aman, Z. M.; McKay, S. F., *Quantitative Ranking and Development of Hydrate Anti-Agglomerants*. In *Offshore Technology Conference Asia*, Offshore Technology Conference: Kuala Lumpur, Malaysia, 2018; 9.

(41) Li, M.; Tian, J.; Liu, C.; Geng, K. Effects of sorbitan monooleate on the interactions between cyclopentane hydrate particles and water droplets. *J. Dispersion Sci. Technol.* **2018**, *39*, 360–366.

(42) Li, M.; Dong, S.; Li, B.; Liu, C. Effects of a naturally derived surfactant on hydrate anti-agglomeration using micromechanical force measurement. *J. Ind. Eng. Chem.* **2018**, *67*, 140–147.

(43) Lee, B. R.; Sum, A. K. Micromechanical cohesion force between gas hydrate particles measured under high pressure and low temperature conditions. *Langmuir* **2015**, *31*, 3884–3888.

(44) Brown, E.; Hu, S.; Wang, S.; Wells, J.; Nakatsuka, M.; Veedu, V.; Koh, C., *Low-Adhesion Coatings as a Novel Gas Hydrate Mitigation Strategy*. Offshore Technology Conference: 2017.

(45) Sghaier, N.; Prat, M.; Ben Nasrallah, S. On the influence of sodium chloride concentration on equilibrium contact angle. *Chem. Eng. J.* **2006**, *122*, 47–53.

(46) Hu, S.; Koh, C. A. Interfacial Properties and Mechanisms Dominating Gas Hydrate Cohesion and Adhesion in Liquid and Vapor Hydrocarbon Phases. *Langmuir* **2017**, *33*, 11299–11309.

(47) Hu, S.; Koh, C. A. CH₄/C₂H₆ gas hydrate interparticle interactions in the presence of anti-agglomerants and salinity. *Fuel* **2020**, *269*, No. 117208.

(48) Frostman, L. M.; Thieu, V.; Crosby, D. L.; Downs, H. H., *Low-Dosage Hydrate Inhibitors (LDHIs): Reducing Costs in Existing Systems and Designing for the Future*. In *International Symposium on Oilfield Chemistry*, Society of Petroleum Engineers: Houston, Texas, 2003; 7.

(49) Frostman, L. M.; Przybylinski, J. L., *Successful Applications of Anti-agglomerant Hydrate Inhibitors*. In *SPE International Symposium on Oilfield Chemistry*, Society of Petroleum Engineers: Houston, Texas, 2001; 10.

(50) Frostman, L. M., *Anti-Agglomerant Hydrate Inhibitors for Prevention of Hydrate Plugs in Deepwater Systems*. In *SPE Annual Technical Conference and Exhibition*, Society of Petroleum Engineers: Dallas, Texas, 2000; 7.

(51) Sun, M.; Firoozabadi, A. New surfactant for hydrate anti-agglomeration in hydrocarbon flowlines and seabed oil capture. *J. Colloid Interface Sci.* **2013**, *402*, 312–319.

(52) Zhao, H.; Sun, M.; Firoozabadi, A. Anti-agglomeration of natural gas hydrates in liquid condensate and crude oil at constant pressure conditions. *Fuel* **2016**, *180*, 187–193.

(53) Kelland, M. A.; Svartaas, T. M.; Øvsthus, J.; Tomita, T.; Chosa, J.-I. Studies on some zwitterionic surfactant gas hydrate anti-agglomerants. *Chem. Eng. Sci.* **2006**, *61*, 4048–4059.

(54) Gao, S. Investigation of Interactions between Gas Hydrates and Several Other Flow Assurance Elements. *Energy Fuels* **2008**, *22*, 3150–3153.

(55) Sanbao Dong, M. L.; Liu, C. Study on the Synergistic Properties of Two Nonionic Natural Gas Hydrate Anti-agglomerants Via Rocking Cell Tests. *Int. J. Energy Power Eng.* **2017**, *6*, 84–90.

(56) Daraboina, N.; Malmos, C.; von Solms, N. Synergistic kinetic inhibition of natural gas hydrate formation. *Fuel* **2013**, *108*, 749–757.

(57) Mehrabian, H.; Bellucci, M. A.; Walsh, M. R.; Trout, B. L. Effect of Salt on Antiagglomerant Surface Adsorption in Natural Gas Hydrates. *J. Phys. Chem. C* **2018**, *122*, 12839–12849.

(58) Gao, S. Hydrate Risk Management at High Watercuts with Anti-agglomerant Hydrate Inhibitors. *Energy Fuels* **2009**, *23*, 2118–2121.

(59) Subramanian, S. *Measurements of clathrate hydrates containing methane and ethane using Raman spectroscopy*. Colorado School of Mines, 2000.

(60) Ballard, A. L. *Non-ideal hydrate solid solution model for a multi-phase equilibria program*, A. Colorado School of Mines. Arthur Lakes Library, 2002.

(61) Monteiro, D.; Multi-Chem, E.; White, J.; Multi-Chem, Z., *Natural Gas Hydrate Management At High Water Cuts By Using Anti-Agglomerant With Thi Supplementation*. 2014.

(62) Costa Salmin, D.; Delgado-Linares, J.; Wu, D. T.; Zerpa, L. E.; Koh, C. A., *Hydrate Agglomeration in Crude Oil Systems in Which the Asphaltene Aggregation State is Artificially Modified*. In *Offshore Technology Conference*, Offshore Technology Conference: Houston, Texas, 2019; 12.

(63) Hu, S. *Interfacial properties of CH₄/C₂H₆ gas hydrate particles with chemical additives*. Colorado School of Mines, Golden, CO, 2019.

(64) Aspenes, G. *The Influence of Pipeline Wettability and Crude Oil Composition on Deposition of Gas Hydrates during Petroleum Production*. University of Bergen, Bergen, 2009.

(65) Opawale, F. O.; Burgess, D. J. Influence of Interfacial Properties of Lipophilic Surfactants on Water-in-Oil Emulsion Stability. *J. Colloid Interface Sci.* **1998**, *197*, 142–150.

(66) Brown, E. P.; Koh, C. A. Micromechanical measurements of the effect of surfactants on cyclopentane hydrate shell properties. *Phys. Chem. Chem. Phys.* **2016**, *18*, 594–600.

(67) Bellucci, M. A.; Walsh, M. R.; Trout, B. L. Molecular Dynamics Analysis of Anti-Agglomerant Surface Adsorption in Natural Gas Hydrates. *J. Phys. Chem. C* **2018**, *122*, 2673–2683.

(68) Jiménez-Ángeles, F.; Firoozabadi, A. Hydrophobic Hydration and the Effect of NaCl Salt in the Adsorption of Hydrocarbons and Surfactants on Clathrate Hydrates. *ACS Cent. Sci.* **2018**, *4*, 820–831.

(69) Bertolazzo, A. A.; Naullage, P. M.; Peters, B.; Molinero, V. The Clathrate–Water Interface Is Oleophilic. *J. Phys. Chem. Lett.* **2018**, *9*, 3224–3231.

(70) Fang, B.; Ning, F.; Hu, S.; Guo, D.; Ou, W.; Wang, C.; Wen, J.; Sun, J.; Liu, Z.; Koh, C. A. The effect of surfactants on hydrate particle agglomeration in liquid hydrocarbon continuous systems: a molecular dynamics simulation study. *RSC Adv.* **2020**, *10*, 31027–31038.

(71) Qi, Y.; Wu, W.; Liu, Y.; Xie, Y.; Chen, X. The influence of NaCl ions on hydrate structure and thermodynamic equilibrium conditions of gas hydrates. *Fluid Phase Equilib.* **2012**, *325*, 6–10.

(72) Dickens, G. R.; Quinby-Hunt, M. S. Methane hydrate stability in seawater. *Geophys. Res. Lett.* **1994**, *21*, 2115–2118.

(73) Mohammadi, A. H.; Afzal, W.; Richon, D. Gas hydrates of methane, ethane, propane, and carbon dioxide in the presence of single NaCl, KCl, and CaCl₂ aqueous solutions: Experimental measurements and predictions of dissociation conditions. *J. Chem. Thermodyn.* **2008**, *40*, 1693–1697.

(74) Ruppel, C.; Dickens, G. R.; Castellini, D. G.; Gilhooly, W.; Lizarralde, D., *Heat and salt inhibition of gas hydrate formation in the northern Gulf of Mexico*. *Geophys. Res. Lett.* **2005**, *32* (4), DOI: 10.1029/2004GL021909.

(75) Moridis, G. J., *Numerical Studies of Gas Production From Methane Hydrates*. In SPE Gas Technology Symposium, Society of Petroleum Engineers: Calgary, Alberta, Canada, 2002; 14.

(76) York, J. D.; Firoozabadi, A. Comparing Effectiveness of Rhamnolipid Biosurfactant with a Quaternary Ammonium Salt Surfactant for Hydrate Anti-Agglomeration. *J. Phys. Chem. B* **2008**, *112*, 845–851.

(77) Dong, S.; Li, M.; Firoozabadi, A. Effect of salt and water cuts on hydrate anti-agglomeration in a gas condensate system at high pressure. *Fuel* **2017**, *210*, 713–720.

(78) Majid, A. A.; Braniff, M.; Creek, J.; Koh, C. A.; Kusinski, G.; Gomes, J., *Gas Hydrate Formation in High Water Content Systems Containing Anti-Agglomerat and Salt*. In Offshore Technology Conference, Offshore Technology Conference: Houston, Texas, USA, 2017; 12.

(79) Sinquin, A.; Arla, D.; Prioux, C.; Peytavy, J. L.; Glenat, P.; Dicharry, C. Gas Hydrate Formation and Transport in an Acidic Crude Oil: Influence of Salt and pH. *Energy Fuels* **2008**, *22*, 721–728.

(80) York, J. D.; Firoozabadi, A. Effect of Brine on Hydrate Antiagglomeration. *Energy Fuels* **2009**, *23*, 2937–2946.

(81) Zyliftari, G.; Lee, J. W.; Morris, J. F. Salt effects on thermodynamic and rheological properties of hydrate forming emulsions. *Chem. Eng. Sci.* **2013**, *95*, 148–160.

(82) Standal, S. H.; Blokhus, A. M.; Haavik, J.; Skauge, A.; Barth, T. Partition Coefficients and Interfacial Activity for Polar Components in Oil/Water Model Systems. *J. Colloid Interface Sci.* **1999**, *212*, 33–41.

(83) Vetráková, L.; Neděla, V.; Runštuk, J.; Heger, D. The morphology of ice and liquid brine in an environmental scanning electron microscope: a study of the freezing methods. *Cryosphere* **2019**, *13*, 2385–2405.

(84) Sloan, D.; Koh, C.; Sum, A. K.; Ballard, A. L.; Creek, J.; Eaton, M.; Lachance, J.; McMullen, N.; Palermo, T.; Shoup, G.; Talley, L., *Natural gas hydrates in flow assurance*. Gulf Professional Publishing: 2010.

(85) Sloan, E. D. Fundamental principles and applications of natural gas hydrates. *Nature* **2003**, *426*, 353–359.

(86) Meng, Z.; Yang, S.-L.; Cui, Y.; Zhong, Z.-Y.; Liang, C.-G.; Wang, L.; Qian, K.; Ma, Q.-Z.; Wang, J.-R. Enhancement of the imbibition recovery by surfactants in tight oil reservoirs. *Pet. Sci.* **2018**, *15*, 783–793.